JACS
JOURNAL OF THE AMERICAN CHEMICAL SOCIETY
Article
pubs.acs.org/JACS

Detection and Electronic Structure of Naked Actinide Complexes: Rhombic-Ring $(AnN)_2$ Molecules Stabilized by Delocalized π-Bonding

Bess Vlaisavljevich,[*,†,‡] Lester Andrews,[*,§] Xuefeng Wang,[∥] Yu Gong,[§] Gary P. Kushto,[⊥] and Bruce E. Bursten[#]

[†]Department of Chemistry, University of Minnesota and Supercomputing Institute, 207 Pleasant St. SE, Minneapolis, Minnesota 55455-0431, United States
[‡]Department of Chemical and Biomolecular Engineering, University of California, Berkeley, California 94720, United States
[§]Department of Chemistry, University of Virginia, P.O. Box 400319, Charlottesville, Virginia 22904-4319, United States
[∥]Department of Chemistry, Tongji University, Shanghai 200092, China
[⊥]United States Naval Research Laboratory, 4555 Overlook Ave SW, Washington, DC 20375, United States
[#]Department of Chemistry and Biochemistry, Worcester Polytechnic Institute, Worcester, Massachusetts 01609-2280, United States

Supporting Information

ABSTRACT: The major products of the reaction of laser ablated and excited U atoms and N_2 are the linear N≡U≡N dinitride molecule, isoelectronic with the uranyl dication, and the diatomic nitride U≡N. These molecules form novel cyclic dimers, $(UN)_2$ and $(NUN)_2$, with complex electronic structures, in matrix isolation experiments, which increase on UV photolysis. In addition, $(NUN)_2$ increases at the expense of $(UN)_2$ upon warming the codeposited matrix samples into the 20−40 K range as attested by additional nitrogen and argon matrix infrared spectra recorded after cooling the samples back to 4 or 7 K. These molecules are identified through matrix infrared spectra with nitrogen isotopic substitution and by comparing the observed matrix frequencies with those from electronic structure calculations. The dimerization is strong (theory predicts the dimer to be on the order of 100 kcal/mol more stable than the monomers), since the ground state involves 12 bonding electrons, 8 in the σ-system, and 4 in the delocalized π-system. This delocalized π bonding is present in the U, Th, La, and Hf analogues further demonstrating the interesting interplay between the 5f and 6d orbitals in actinide chemistry. The $(UN)_2^+$ cation is also observed in solid argon, and calculations indicate that the bonding in the ring is preserved. On the other hand, the NUN dimer is of lower C_{2h} symmetry, and the initial NUN molecules are recognizable in this more weakly bonded ($\Delta E = -64$ kcal/mol) structure. The NThN molecules bind more strongly in the $(NThN)_2$ dimer than the NUN molecules in $(NUN)_2$ since NUN itself is more stable than NThN.

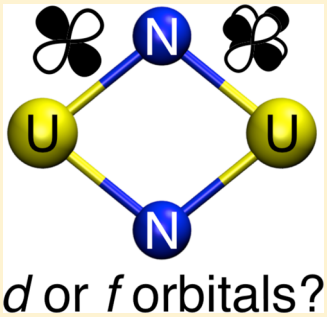

INTRODUCTION

Nuclear energy plays an essential role in global energy production, and therefore understanding the chemistry of uranium is essential in the development of a truly efficient nuclear energy cycle. Nevertheless fundamental questions regarding the nature of uranium ligand bonds remain. Valuable insights have been provided through spectroscopic and theoretical studies of actinide-containing systems, but much of this work has focused on more common uranium compounds, in particular those with uranium−oxygen bonds. While uranium nitrogen bonds are known and uranium nitrogen fuel sources have often been cited as an alternative to current oxide fuels, only three uranium nitride solids have been characterized (UN, UN_2, and U_2N_3).[1,2]

However, a few molecular species containing terminal uranium nitride groups have been produced and identified through efforts involving matrix isolation experiments as well as traditional coordination chemistry.[3] Using matrix isolation to probe the nature of the coordination chemistry of uranium has proven successful, in particular for the well-studied uranium oxides. However, reactions of laser ablated uranium atoms with small molecules have led primarily to single uranium-atom-bearing products.[4−10] For example, the reaction of uranium with O_2 in excess argon gave UO_2 as the major product and UO and UO_3 as minor products, all in agreement with earlier evaporative work from solid UO_2 near 2000 °C.[8,11] Likewise, subsequent investigations using excess neon identified UO_2 in the $^3\Phi$ ground state and UO_2^+ in the $^2\Phi$ ground state.[10] Returning to reactions of uranium with N_2, the major product observed in the argon matrix infrared spectrum from the reaction of laser ablated and excited U atoms with N_2 is the insertion dinitride, N≡U≡N, and a small amount of the diatomic uranium nitride U≡N.[12−15] These molecules were first detected by Green and Reedy from sputtering argon/nitrogen mixtures through a hollow uranium cathode and condensing the effusing gas for spectroscopic analysis.[16] When pure nitrogen was employed as both reagent and matrix, large

Received: October 14, 2015
Published: December 8, 2015

DOI: 10.1021/jacs.5b10458
J. Am. Chem. Soc. 2016, 138, 893−905

yields of both NUN and UN were observed saturated with N_2 ligands.[14,17] Moreover, multiple bonding between U and N in simple new molecules was found in reactions of U with N_2 and H_2 mixtures in our laboratory that produced the N≡U═N−H molecule containing both triple and double uranium−nitrogen bonds, as characterized by the infrared spectrum and theoretical calculations.[7] Additionally, high-level calculations have been performed for uranium triatomic compounds XUY (X,Y ═C, N, and O).[18] As expected, the reaction of U and NF_3 did produce the most stable N≡UF_3 product,[4] but the reaction with NH_3 yielded mostly HN═UH_2, and CH_4 gave CH_2═UH_2.[5,7,19] The most important recent information in the terminal nitride UN genre comes from rotationally resolved optical transitions of uranium nitride, also produced by laser ablation, which provided a ground-state UN bond length of 1.7650(12) Å and proposed that UN could be considered as $U^{3+}N^{3-}$.[20] Additionally, the spectroscopy and structure of the simplest actinide bonds have been recently reviewed by Heaven et al.[21]

On the other hand, terminal uranium nitrides are a very challenging target for synthetic chemists and have only recently been reported.[22−24] Additionally, species containing R−UN subunits have been characterized, which include numerous intramolecular interactions that are not present in the matrix isolation studies; therefore, the spectroscopic behavior of this −UN subunit may vary from system to system.[25−29] Additionally, uranium−nitrogen bonding has been investigated in uranium nitride complexes featuring a linear U−N−U core[30] as well as for uranium dinitrogen complexes stabilized by supporting ligands.[31] While this work only explores uranium−nitrogen complexes, it should be noted that Schmidt et al. recently synthesized a dinuclear bis-μ-oxo with a diamond core motif.[32]

The purpose of this paper is to identify the isolated $(UN)_2$ molecule in the absence of strongly perturbing ligands and to characterize the unique bonding offered by six bonding orbitals in $(UN)_2$ through electronic structure calculations. The high symmetry of the molecule, in conjunction with our experience in the relative participation of U 5f and 6d orbitals in bonding, allows us to use qualitative descriptions that clarify the quantitative calculations to provide a clearer picture of the bonding within the rhombic ring. In addition, we seek evidence for the dimer of NUN and explore its bonding properties. We have previously investigated three other uranium-bearing molecules to offer as benchmarks, HU−NH_2, H_2U═NH, and H−N═U≡N.[4,7] By using conditions that result in a large yield of UN, the possibility of observing its dimer $(UN)_2$ is increased, and new bands are assigned to the antisymmetric stretching modes of the rhombic $(UN)_2$ molecule in solid argon without saturating N_2 ligands on the basis of their higher vibrational frequencies and their unique $^{14}N/^{15}N$ isotopic frequency ratios. Finally, comparisons with bonding in the Th, La, Hf, and W analogues are made to illuminate further the unique bonding in $(UN)_2$.

EXPERIMENTAL AND COMPUTATIONAL METHODS

Matrix Isolation Spectroscopy. Our apparatus and techniques for investigating the matrix infrared spectra of new uranium-bearing molecules have been described in previous publications.[14,33] In this work, laser-ablated U atoms were reacted with N_2 in excess argon or nitrogen during condensation at 4 or 7 K using methods reported recently.[14,17] The Nd:YAG laser fundamental (1064 nm, 10 Hz repetition rate with 10 ns pulse width) was focused onto a rotating uranium metal target (Oak Ridge National Laboratory, high purity, ^{238}U depleted of ^{235}U). Isotopic samples of molecular nitrogen diluted in argon were prepared in a stainless steel vacuum line. Pure nitrogen isotopic samples were also codeposited with U atoms. Selected samples were passed through a 6 mm o.d. quartz tube with a 1−2 mm orifice and subjected to microwave discharge during deposition with U atoms. Then FTIR spectra were recorded at 0.5 cm^{-1} resolution on a Nicolet 750 with 0.1 cm^{-1} accuracy using an HgCdTe range B detector. Samples were alternatively subjected to glass filtered Hg-arc street lamp irradiation (Philips, 175 W) and temperature cycled, i.e., annealed.

DFT and Wave Function-Based Methods. Quantum chemical calculations included both density functional and high-level wave function-based methods. Geometry optimizations were performed using the B3LYP density functional and the 6-311+G(3df) basis set for N, while the small core SDD pseudopotential was used for uranium along with an optimized (12s11p10d8f) [8s7p6d4f] Gaussian valence basis set.[34−37] Mayer bond orders were also computed.[38,39] While this level of theory has been used previously with much success, the choice of B3LYP as the functional has been tested against the meta GGA M06-L for U, N, UN, NUN, and $(NUN)_2$ to ensure that this was the case for the systems studied herein.[40] All density functional theory (DFT) calculations were preformed with the Gaussian 09 software package.[41] To study the electronic structure in further detail, complete active space self-consistent field calculations with corrections from second-order perturbation theory (CASSCF/CASPT2) were performed.[42−44] The choice of active space is given in detail in the following; however, in order to properly account for the bonding in $(UN)_2$, the number of so-called active orbitals and electrons required was more than is feasible within the CASSCF formalism. Therefore, restricted active space SCF with corrections from second-order perturbation theory (RASSCF/RASPT2) calculations were performed.[45,46] Scalar relativistic effects were treated through the use of the Douglas−Kroll−Hess (DKH) Hamiltonian,[47,48] and ANO-RCC basis sets of triple-ζ quality were employed with the following contractions: 9s8p6d4f2g1h for uranium and thorium, 8s7p5d2f1g for lanthanum, 8s7p5d3f2g for tungsten and hafnium, and 4s3p2d1f for nitrogen.[49,50] CASPT2 and RASPT2 calculations were performed as implemented in the Molcas 7.9 software package.[51] Cholesky decomposition was used in combination with local exchange (LK) screening to reduce the cost of the two electron integrals.[52−55] Note that spin orbit coupling was not included in the calculations. While we do not except the bonding picture that emerges, we were unable to compute enough excited states to properly determine the spin−orbit contribution given the large size of the active spaces required for $(AnN)_2$ species. Finally, CCSD(T) calculations were performed using the aug-cc-PVTZ basis sets of Peterson and co-workers[56] to compute the thermochemistry for the formation of $(NUN)_2$ at a higher level of theory as implemented in the Molpro software package.[57,58]

RESULTS AND DISCUSSION

The major product in the reaction of laser ablated and excited U atoms with N_2 is NUN, and UN is a minor product.[14,17] When nitrogen is used as the matrix as well as the reagent, a higher yield of NUN and UN is produced, but the higher complexes $NU(NN)_6$ and $NUN(NN)_5$ are also formed. However, when enough UN and NUN are present, dimerization can occur. The dimer $(UN)_2$ has been observed in solid nitrogen, and another species, assigned first as $N(UN)_2$, will be reassigned below to $N(UN)_2N$ ((hereafter the NUN dimer $(NUN)_2$).[16] Matrix infrared spectra of uranium and nitrogen reaction products will be analyzed paying particular attention to ^{14}N and ^{15}N isotopic spectra and comparisons with harmonic frequencies from electronic structure calculations for potential products and their N_2 (hereafter noted NN) complexes. The bonding in and structure of cyclic $(UN)_2$-bearing molecules are the subject of this report, which will be

DOI: 10.1021/jacs.5b10458
J. Am. Chem. Soc. 2016, 138, 893−905

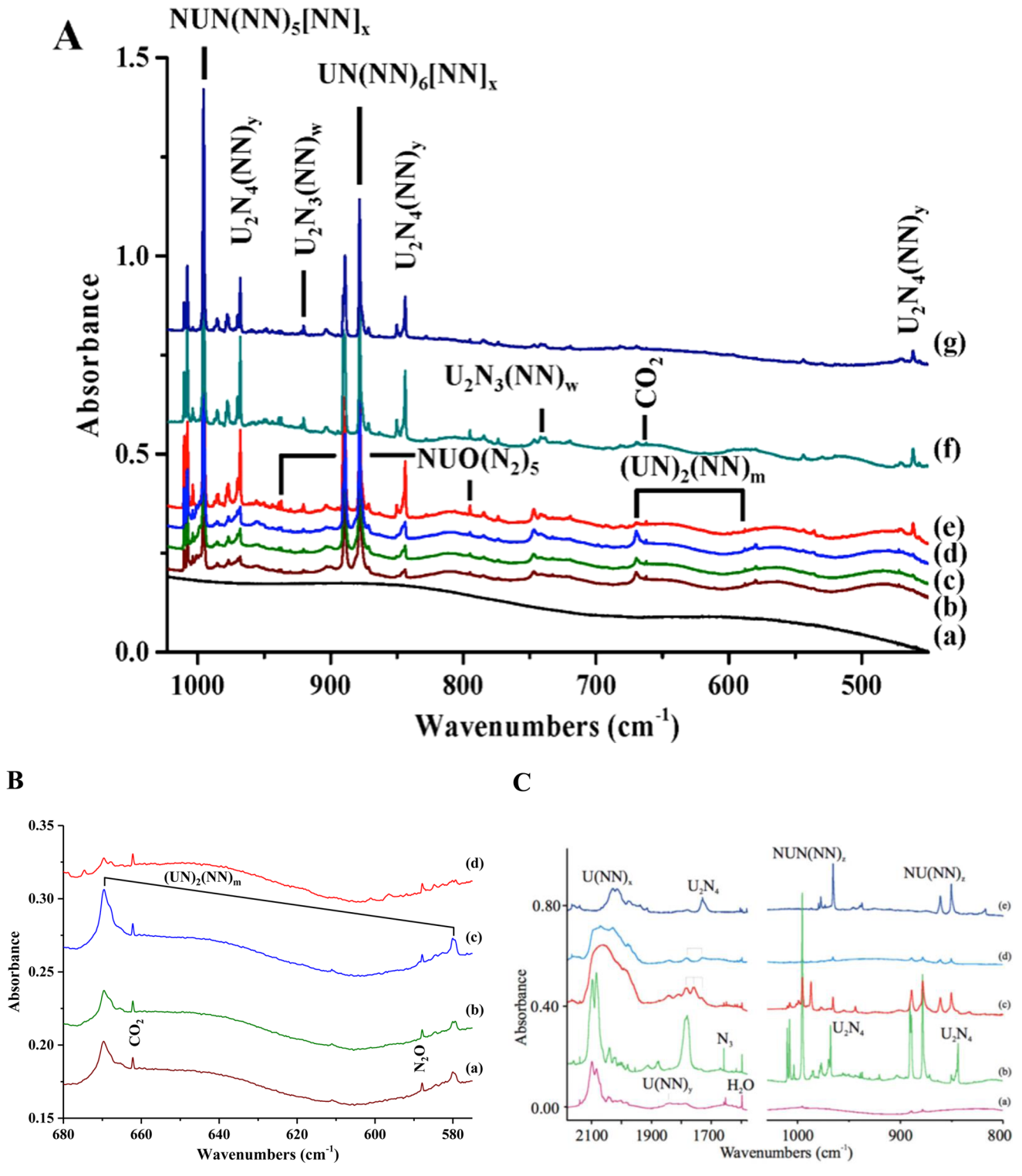

Figure 1. (A) Nitrogen matrix spectra of laser ablated U reaction products with the matrix molecules. (a) Nitrogen gas passed through the microwave discharge (the N_3 radical absorption at 1657.5 cm^{-1} as reported by Tian et al. is not shown).[60] (b) Laser ablated U codeposited with nitrogen gas passed through the microwave discharge, (c) after annealing to 20 K, (d) after annealing to 25 K, (e) after >220 nm irradiation for 15 min, (f) after annealing to 30 K, and (g) after annealing to 35 K. (B) Expanded frequency scale for nitrogen matrix spectra of laser ablated U reaction products with the matrix molecules. (a) Laser ablated U codeposited at 7 K with nitrogen gas passed through the microwave discharge for 1 h, (b) after annealing to 20 K, (c) after >220 nm irradiation for 15 min, and (d) after annealing to 30 K. (C) Infrared spectra of the N−N and U−N stretching regions for laser ablated uranium and nitrogen reaction products upon codeposition in pure isotopic nitrogen at 4 K. (a) U and $^{14}N_2$ codeposited for 30 min with low power microwave discharge of the depositing nitrogen sample, (b) U and $^{14}N_2$ codeposited for 60 min with higher power microwave discharge, (c) U and $^{14}N_2$ and $^{15}N_2$ 50/50 mixture codeposited with higher power discharge, (d) U and $^{14}N_2$ and $^{15}N_2$ 50/50 mixture codeposited with no discharge hence no $^{14}N^{15}N$ is produced, and (e) U and $^{15}N_2$ codeposited with higher power discharge. There is another absorption at 461.0 cm^{-1} that shifts to 446.8 cm^{-1} with $^{15}N_2$ and gives a triplet structure with the scrambled isotopic sample in spectrum (c).

DOI: 10.1021/jacs.5b10458
J. Am. Chem. Soc. 2016, 138, 893−905

Table 1. Observed and B3LYP Calculated Vibrational Frequencies in cm^{-1} with Their Corresponding Intensities in Parentheses in Units of km/mol[a]

molecule	^{14}N exp	^{14}N calculated	^{15}N exp	^{15}N calculated	mode description
UN	1001.1[b]	1037.2 (215)	969.5	995.4 (182)	U≡N stretch
NUN	1050.9[c]	1111.7 (566)	1019.4	1078.1(532)	N≡U≡N antisymmetric stretch
		209.4 (20) B_{1u}		202.7 (19)	out of plane deformation
		213.6 (0) A_g		213.4 (0)	
		398.8 (0) B_{1g}		385.8 (0)	U−N symmetric stretch
U_2N_2 or $(UN)_2$ $^7B_{1u}$	580.2[d]	607.9 (159)[d] B_{3u}	561.7	588.5 (149)	U−N antisymmetric stretch, B_{3u}
	669.6[d]	647.8 (1841)[d] B_{2u}	648.6	627.1 (1726)	U−N antisymmetric stretch, B_{2u}
		696.7 (0)[d] A_g		673.6 (0)	U−N symmetric stretch
		13.3 (34)		12.3 (32)	
		81.1 (25)		78.6 (24)	
		210.9 (39)		204.1 (37)	
		213.2 (0)		212.9 (0)	
U_2N_3 or $N(UN)_2$ ^3A		334.1 (0)		323.1 (0)	U−N symmetric stretch
		600.9 (175)		581.8 (165)	U−N antisymmetric stretch
		700.7 (166)		677.5 (147)	U−N symmetric stretch
	742.2	739.5 (324)	719.3	715.3 (309)	U−N antisymmetric stretch
	920.6	1048.4 (416)	891.9	1015.0 (395)	U≡N stretch
		74.7 (62)		72.3 (58)	
		95.2 (0)		92.5 (0)	
		114.1 (59)		110.4 (55)	
		117.1 (0)		113.9 (0	
		159.4 (0)		158.8 (0)	
		242.6 (96)		235.0 (91)	
U_2N_4, $N(UN)_2N$, or $(NUN)_2$ $^1A_1$		434.5 (0)		420.5 (0)	U−N symmetric stretch
	461.5[e]	474.0 (275)	446.9	459.0 (259)	U−N antisymmetric stretch
		779.5 (0)		754.0 (0)	U−N symmetric stretch
	843.8[e]	881.7 (590)	816.9	853.3 (543)	U−N antisymmetric stretch
	968.0[e]	1071.6 (718)	937.5	1037.5 (687)	U≡N antisymmetric stretch
		1082.9 (0)		1048.6 (0)	U≡N symmetric stretch

[a]The experimental values for UN and NUN were measured in solid argon at 4 K, and the cyclic species $(UN)_2$, $N(UN)_2$, and $(NUN)_2$ were measured in a solid nitrogen at 7 K. When other labels have been used previously, those labels have been included as well. [b]Frequency for the saturated $NU(NN)_6[NN]_x$ complex is 878.2 cm^{-1} in solid nitrogen. [c]Observed $^{14}NU^{15}N$ frequencies 1040.7 and 987.2 cm^{-1} for the linear molecule in solid argon. Frequency for the saturated $NUN(NN)_5[NN]_x$ complex is 995.7 cm^{-1} in solid nitrogen. [d]Observed $(U^{14,15}N)_2$ frequencies are 659.6 and 569.8 cm^{-1} in solid nitrogen. The B3LYP calculated values for the $^{14/15}N$ isotope are 206.1 (20), 213.5 (0), 392.0 (1), 596.9 (151), 637.8 (1783), and 686.4 (3). The argon matrix counterparts are 705.6, 695.0, and 683.5 cm^{-1}. [e]Observed mixed 14/15 frequencies are 968.0 and 937.5 cm^{-1}, 843.8, 831.8, and 816.9 cm^{-1}, and 461.0, 456.4, and 446.8 cm^{-1}.

described by both DFT and high-level wave function-based calculations. (The activation energy (*) required to initiate reactions 1 and 2 is not included in the energy changes.)

$$U^* + N_2 \rightarrow NUN \quad \begin{array}{l} \text{B3LYP, } \Delta E = -68 \text{ kcal/mol} \\ \text{M06-L, } \Delta E = -85 \text{ kcal/mol} \\ \text{CASPT2, } \Delta E = -73 \text{ kcal/mol} \end{array} \quad (1)$$

$$U^* + N_2 \rightarrow N + UN \quad \begin{array}{l} \text{B3LYP, } \Delta E = +103 \text{ kcal/mol} \\ \text{M06-L, } \Delta E = +77 \text{ kcal/mol} \\ \text{CASPT2, } \Delta E = +98 \text{ kcal/mol} \end{array} \quad (2)$$

Infrared Spectra of Uranium and Nitrogen Reaction Products in Pure Nitrogen. The U and NN reaction products in pure nitrogen exhibit intensities over a 100-fold range from the very intense sharp 995.7 cm^{-1} band assigned to the $NUN(NN)_5[NN]_x$ complex, where x defines the saturated secondary coordination layer around the pentagonal bipyramidal $NUN(NN)_5$ core complex to weaker and lower frequency bands at 669.6, and 580.2 cm^{-1} identified as the rhombic $(UN)_2(NN)_y$ complex, where y notes an unknown number of NN ligands. The second strongest bands identified previously at 890.5 and 878.2 cm^{-1} were assigned to UN dinitrogen complexes with the lower band due to the saturated $NU(NN)_6[NN]_x$ complex.[14,59] Since we are looking for diuranium product species, it follows that dimers formed from the major NUN and UN product complexes are in order, so we will consider new bands in the pure nitrogen matrix experiments first, which are illustrated in Figure 1A–C. The first scan (a) shows the NN matrix in the absence of uranium. The second scan (b) features a similar NN sample codeposited with laser ablated U atoms, and the above-described very strong NUN and UN complex absorptions stand out from the rest. We now wish to focus on three separate additional species: four bands at 1785, 968.0, 843.8, and 461.5 cm^{-1} (labeled $U_2N_4(NN)_y$, new bands at 920.6 and 742.2 cm^{-1} (denoted $U_2N_3(NN)_w$, and the two lower frequency bands at 669.6 and 580.2 cm^{-1} (identified as $U_2N_2(NN)_m$) will be assigned to these three $(UN)_2$-bearing species.

DOI: 10.1021/jacs.5b10458
J. Am. Chem. Soc. 2016, 138, 893–905

Figure 1A illustrates infrared spectra for experiments using natural isotopic nitrogen as matrix and reagent. The first scan (a) shows the spectrum for discharged nitrogen without U, and the only band of interest is that for N_3 radical at 1657.5 cm^{-1} as cited above. This shows that N atoms are deposited in the nitrogen gas stream. When laser ablated U was included, very intense bands are observed for $NUN(NN)_x$ complexes at 1010.2, 1007.8, and 995.7 cm^{-1} as well as at 890.5 and 878.2 cm^{-1} for $NU(NN)_{5,6}$ complexes.[14,59] Weaker bands at 669.6 and 580.2 cm^{-1} were assigned to $(UN)_2$ based on their $^{14}N/^{15}N$ isotopic frequency ratios and the observation of triplet isotopic patterns using scrambled mixed reagent $^{14,15}N_2$, which indicates two equivalent nitrogen atoms.[17] A dinuclear rhombus structure was suggested even though PW91 density functional calculations found a puckered ring. Figure 1B focuses on the 680 to 580 cm^{-1} region of the spectra. First, the two band profiles are similar in that lower frequency shoulders are observed at 667.8 on the major 669.6 cm^{-1} band and at 579.5 on the lower 580.2 cm^{-1} peak. Next, notice that these two absorptions decrease slightly in intensity together upon annealing to 20 K, while three other absorptions in Figure 1A at 968.0, 843.8, and 461.5 cm^{-1} double in intensity (observation of the latter requires expanded absorbance scale) and weak bands at 920.5 and 742.2 cm^{-1} increase slightly. Then full-arc photolysis [>220 nm] almost doubles the 669.6 and 580.2 cm^{-1} bands and increases the 968.0, 843.8, and 461.0 cm^{-1} absorptions by 30%. Annealing the sample to 30 K reduces the $(UN)_2$ bands by 75% and increases the 920.6 cm^{-1} band 3-fold and the 968.0, 843.8, and 461.5 cm^{-1} absorptions 4-fold. Annealing to 35 K has little effect on the $(UN)_2$ bands, but increases the 920.6 cm^{-1} band by 50% and the 968.0, 843.8, and 461.5 cm^{-1} absorptions by 30%. Final annealing to 40 K decreases all of these absorptions as shown in Figure 1A(g).

Similar experiments without microwave discharge of the nitrogen stream gave similar spectra with lower product yields, and sample deposition at 4 K also reduced the product yields. As expected, experiments with lower laser energy gave lower product yields but more growth on initial photolysis. In such an experiment, irradiation of the freshly deposited sample increased the $(UN)_2$ bands 5-fold and doubled the 968.0, 843.8, and 461.5 cm^{-1} absorptions. Annealing to 20, 30, and 35 K decreased and removed the 669.6 and 580.2 cm^{-1} bands and increased the 920.5 and 744.2 cm^{-1}, and the 968.0, 843.8, and 461.5 cm^{-1} absorptions by a factor of 4.

Additional experiments were performed with nitrogen-15 substituted gas and mixtures of $^{14}N_2$ and $^{15}N_2$ gas and scrambled $^{14}N_2/^{14}N^{15}N/^{15}N_2$ gas samples. The higher frequency region is shown in Figure 1C, while the $^{15}N_2$ product frequencies are given in Table 1. The absorptions had the same profile and splittings as shown in Figure 1B. No intermediate components were observed with the mixed $^{14}N_2$ and $^{15}N_2$ reagents, but the upper peaks were shifted together by 0.2 cm^{-1} to 669.4 and 648.8 cm^{-1}: This shows the effect of the isotopic host matrix and higher complexes with isotopic NN molecules in the complexes formed. Finally, the scrambled isotopic mixture gave additional mixed $^{14}N^{15}N$ isotopic products, and these absorptions did not have the shoulder peak below the main bands like the $^{14}N_2$ and $^{15}N_2$ isotopic molecules.

Infrared Spectra of Uranium and Nitrogen Reaction Products in Solid Argon. Likewise, the $NUN(NN)_{0-5}$ and $NU(NN)_{0-6}$ molecules and complexes absorbing at 1050.9−995.0 cm^{-1} and 1001.1−935.6 cm^{-1} have been identified in a solid argon matrix,[12−14] and we want to now focus on the lower frequency region where bridging N−U−N stretching vibrations are expected. In our recent work, we noted new absorptions at 828 and 699 cm^{-1} with an asterisk (*) to indicate species with more than one U atom based on relative metal concentration;[14] however, these will not be considered here owing to the fact that mixed nitrogen isotopic spectra suggest the presence of only one N atom, ruling them out for $(UN)_2$-bearing species. Based on the behavior of NUN and UN, we expect the argon matrix isolated species to exhibit higher frequencies than the nitrogen matrix values, and we begin with the region just above the nitrogen matrix frequencies.

The $(NUN)_2$ species has the strongest frequencies, so we search at 843 cm^{-1} with 0.5% N_2 in argon in Figure 1 of our recent paper.[14] These spectra exhibit a weak, sharp band at 847 cm^{-1} that increases on annealing to 30 and to 35 K and then decreases on annealing to 45 K, which is similar to the behavior of the 843.8 cm^{-1} band in Figure 1A herein. Unfortunately, the 970 cm^{-1} region is covered by UN complex absorptions. A weak band at 925.3 cm^{-1} increases during the annealing cycles.[14]

The 760−440 cm^{-1} region from this experiment is illustrated in Figure 2. The most important bands are at 705.6, 621.7, and

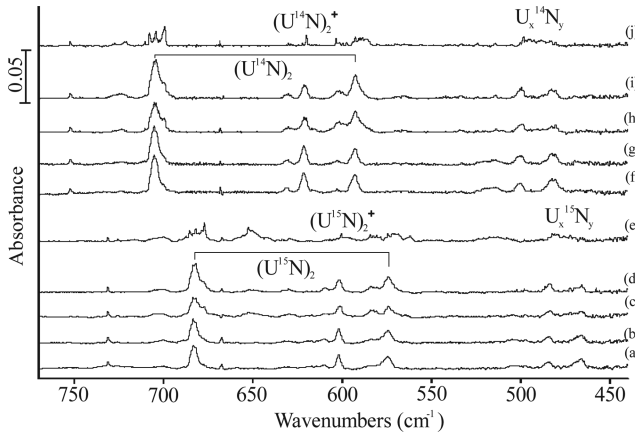

Figure 2. Infrared spectra in the lower frequency region for laser ablated U and 0.5% N_2 reaction products in solid argon at 4 K. Five spectra at the bottom (a, b, c, d, e) are from sample codeposition for 60 min using $^{15}N_2$, annealing to 20 K, annealing to 30 K, UV > 220 nm photolysis for 20 min, and annealing to 40 K. Five spectra at the top (f, g, h, i, j) are from the same treatments for $^{14}N_2$.

593.0 cm^{-1}. Annealing to 30 K decreased these bands, and UV photolysis increases the 705.6 and 593.0 cm^{-1} pair with no effect on the 621.7 cm^{-1} band. Spectra from a similar experiment with $^{15}N_2$ are also shown in Figure 2, where the obvious shifted counterparts are at 683.5, 602.1, and 574.4 cm^{-1}. Spectra from a statistical $^{14,15}N_2$ sample gave triplet absorptions with the above bands plus intermediate components at 695.5, 610.3, and 584.9 cm^{-1}. Next we examine Figure 4 of our previous work with 2.5% N_2 in argon,[14] and we find weak bands which increase at 971.7 and 844.7 cm^{-1} on the annealing cycles. Weak bands were observed at 705.6, 621.7, and 593.0 cm^{-1}, which increased slightly on UV photolysis. These bands decreased on annealing in favor of bands at 672 and 586 cm^{-1}. Finally, a 10% N_2 experiment with 90% argon, Figure 2 from previous work,[13] annealing to 20 K produces weak bands at 971.3 and 845.1 cm^{-1}, then annealing to 30 K increases these bands and shifts them lower to 970.5 and 844.9

DOI: 10.1021/jacs.5b10458
J. Am. Chem. Soc. 2016, 138, 893−905

cm^{-1} followed by annealing to 40 K which increases and shifts these bands to 970.0 and 844.5 cm^{-1} and a peak appears at 462.5 cm^{-1}. This annealing sequence also produced a new band at 924.0 to 923.5 to 922.6 cm^{-1}, which relates to the 920.6 cm^{-1} band in solid nitrogen. These spectra also show new bands at 671 and 585 cm^{-1} on photolysis, which slightly increase on annealing to 20 K. However, no 621.7 cm^{-1} band was observed. The analogous experiment with 8% $^{15}N_2$ and 92% argon gave stronger counterparts at 651 and 567 cm^{-1}. Finally, peaks were observed at 515.0, 500.7, and 482.4 cm^{-1} on top of a broad band that decreased on annealing (see Figure 2). These features have larger nitrogen-15 shifts (14/15 frequency ratios 1.033), which indicates more N motion than the above products and suggests the possibility of even higher uranium nitride species.[14]

Identification of $(UN)_2$. The triplet isotopic patterns reported earlier for the $^{14}N_2/^{14}N^{15}N/^{15}N_2$ isotopic spectra demonstrated the presence of two equivalent N atoms in this reaction product, and the UN diatomic monomer isotopic shifts suggested a rhombus dimer structure.[16] The NUN contributes the higher frequency band at 995.7 cm^{-1}, with a lower $^{14}N/^{15}N$ isotopic frequency ratio 1.0312, so we are drawn to the rhombus structure. The isotopic frequencies have been measured again, and they are listed in Table 1. The two absorptions at 669.6 and 580.2 cm^{-1} have almost the same $^{14}N/^{15}N$ isotopic frequency ratios, 1.0324 and 1.0329, which are very close to the 1.0326 ratio for the UN diatomic molecule and clearly higher than that for NUN.[14,16] The rhombus is the only plausible structure, Figure 3, which gives the same isotopic

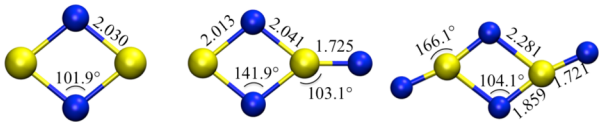

Figure 3. Comparison of select geometric parameters for $(UN)_2$, $N(UN)_2$, and $(NUN)_2$ at the B3LYP level of theory. Distances are given in Å and angles in degrees. The color scheme is as follows: uranium in yellow and nitrogen in blue.

frequency ratio for two antisymmetric stretching fundamentals, which have the special relationship of diatomic molecule isotopic frequency ratios as shown in the G-matrix elements for the rhombic $(LiO)_2$ molecule by White et al.[61] The 669.6 and 580.2 cm^{-1} bands in solid nitrogen are assigned to the B_{2u} and B_{3u} antisymmetric stretching modes of the $(UN)_2$ rhombic ring, which are calculated at 647.8 and 607.9 cm^{-1} with B3LYP for this septet ground-state molecule of multireference character (Table 1). This is good agreement particularly in view of the presence of dinitrogen ligands in the nitrogen matrix environment. Notice that our calculation finds zero intensities for the three *gerade* modes and an approximately 12/1 intensity ratio for the B_{2u} and B_{3u} modes, which is in good agreement with integrated absorbance ratio measurements of 7/1 and 8/1 in spectra from two different experiments. The argon matrix counterparts were higher in frequency at 705.6 and 593.0 cm^{-1} with almost the same $^{14}N/^{15}N$ isotopic frequency ratios, 1.0323 and 1.0324. The neon matrix counterpart of the stronger, higher frequency band was observed at 709.8 cm^{-1}.[14]

Additional Supporting Information for the rhombus (D_{2h}) assignment can be taken from the observed and computed frequencies of the $(U^{14}NU^{15}N)$ mixed isotopic molecule, which has a G matrix that displays lower (C_{2v}) symmetry. The $(U^{14}NU^{15}N)$ isotopic counterparts for the two antisymmetric modes are observed at 659.6 and 569.8 cm^{-1}, which are 0.5 cm^{-1} above the 659.1 cm^{-1} average for the higher modes of $(U^{14}N)_2$ and $(U^{15}N)_2$ and 1.2 cm^{-1} below the 571.0 cm^{-1} average for the lower modes of $(U^{14}N)_2$ and $(U^{15}N)_2$. This increased separation arises because of different interactions among the modes now of lower symmetry. Almost the same relationship is shown in the calculated frequencies (Table 1), where the mixed isotopic frequencies are 0.4 cm^{-1} above and 1.3 cm^{-1} below the averages of the $(U^{14}N)_2$ and $(U^{15}N)_2$ values.

As we dilute the nitrogen matrix with argon, the above bands increase: Using 10% $^{14}N_2$ sample, bands for $(^{14}UN)_2$ in solid argon are at 671 and 585 cm^{-1} and with $^{15}N_2$ counterparts at 651 and 567 cm^{-1}. The $^{14}N/^{15}N$ isotopic frequency ratios are 1.031 and 1.032, which are close to the diatomic UN values. We suspect that there are some NN ligands associated with these rhombic molecules owing to the relatively high 10 and 8% reagent concentrations in excess argon. These argon matrix bands are blue-shifted only by 3−5 cm^{-1} from the pure nitrogen matrix values in contrast with the much larger shifts observed for NUN and UN, 55 and 123 cm^{-1}, respectively, on going from argon to the full nitrogen matrix environment.

In the nitrogen matrix experiments the 669.6 and 580.2 cm^{-1} bands of $(UN)_2$ decrease on annealing in favor of both the 920.6 and associated 742.2 cm^{-1} bands and the 968.0, 843.8, and 461.5 cm^{-1} set. Such behavior shows that the former pair is due to a reactive species. This is all consistent with the diffusion and reaction of trapped N atoms as attested by the observation of the N_3 radical in the initial frozen sample,[61] and assignment of these latter bands to species chemically related to $(UN)_2$ will be made below.

Identification of $(UN)_2^+$. The sharp 621.7 cm^{-1} argon matrix band exhibits a 602.1 cm^{-1} $^{15}N_2$ counterpart with a 1.0326 $^{14}N/^{15}N$ diatomic UN isotopic frequency ratio and a sharp 610.3 cm^{-1} mixed $^{14}N^{15}N$ isotopic component; all of these observations are appropriate for two equivalent N atoms and a rhombus structure. The strongest computed frequency for the rhombic ring cation, Figure 4, is at 630.2 cm^{-1}, which is

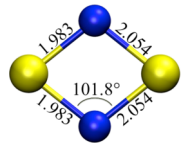

Figure 4. Select geometric parameters and calculated frequencies for the sextet ground state of $(UN)_2^+$ at the B3LYP level of theory. Distances are in Å and angles in degrees. The color scheme is as follows: uranium in yellow and nitrogen in blue. The U−U distance is 3.132 Å. B3LYP frequencies (cm^{-1}) and intensities given in parentheses (km/mol) for the sextet ground state are 186.1 (4), 206.5 (27), 398.5 (9), 462.3 (0), 630.2 (164), and 740.4 (0).

in excellent agreement with our 621.7 cm^{-1}argon matrix band and thus supports the cation assignment. The calculated $^{15}N_2$ counterpart at 610.1 cm^{-1} gives a 1.0329 isotopic frequency ratio that is slightly higher than the observed value owing to anharmonicity. The laser ablation plume contains sufficient vacuum UV radiation to produce cations in this chemical system, as the observation of UO_2^+ in previous argon and neon matrix experiments with oxygen demonstrates.[10,62] It is thus noteworthy that the 621.7 cm^{-1} band increases 4-fold relative to the $(UN)_2$ bands when the 0.5% N_2 in argon reagent stream

DOI: 10.1021/jacs.5b10458
J. Am. Chem. Soc. 2016, 138, 893−905

Table 2. Select Geometric Parameters for Uranium Nitride Species Computed at the B3LYP Level of Theory[a]

	U≡N	U=N	U−N	U−N−U angle
UN	1.758 (2.43)	–	–	–
NUN	1.723 (2.15)	–	–	–
$(UN)_2$	–	2.030 (1.22)	–	101.9
$N(UN)_2$	1.725 (2.20)	2.013/2.041 (1.23)	–	141.9
$(NUN)_2$	1.721 (2.13)	1.859 (1.50)	2.281 (0.75)	104.1
$(UN)_2^+$		1.983/2.054	–	101.8
HN=U≡N[b]	1.741	1.931	–	–
H−U−NH_2[c]	–	–	2.193	–
HN=UH_2[c]	–	1.903	–	–

[a]Distances are in Å and angles in degrees. Mayer bond orders are given in parentheses for the species studied in this work. [b]Ref 7. [c]Ref 5.

is subjected to microwave discharge during sample deposition with the discharged gas effusing out the tube orifice, which can be expected for the absorption of a trapped ion. The 621.7 cm^{-1} cation absorption is observed in the 2.5% N_2 experiment, but annealing broadens it to 618 cm^{-1}. This cation absorption is not observed with 10% N_2 in argon nor with pure nitrogen, as surely it is a very reactive species. Laser ablation also produces U^+ ions,[10] and the reaction 3 with NUN is a likely route for the formation of $(UN)_2^+$. Finally, the $(UN)_2^+$ cation is a sufficiently stable species to expect mass spectroscopic detection under thermal decomposition of uranium nitride solids.[1,2]

$$U^+ + NUN \rightarrow (UN)_2^+ \quad \text{B3LYP, } \Delta E = -117.6 \text{ kcal/mol} \tag{3}$$

Identification of $(NUN)_2$. The pronounced growth of the 968.0, 843.8, and 461.5 cm^{-1} bands at the expense of $(UN)_2$ upon annealing the spectra in Figure 1 to 30−35 K invites consideration of two N atom addition species through reactions 4 and 5.

$$N + (UN)_2 \rightarrow N(UN)_2 \quad \text{B3LYP, } \Delta E = -131.3 \text{ kcal/mol} \tag{4}$$

$$N + N(UN)_2 \rightarrow N(UN)_2N \quad \text{B3LYP, } \Delta E = -130.4 \text{ kcal/mol} \tag{5}$$

The two lowest above absorptions yield 1/2/1 mixed isotopic triplets using the scrambled $^{14,15}N_2$ isotopic reagent, which indicates the participation of two equivalent and coupled N atoms in these two vibrational modes like in a rhombic ring. The higher band at 968.0 cm^{-1} revealed only a mixed isotopic ^{14}N and ^{15}N doublet, which would normally indicate a single N atom, but this could also be the signature of two equivalent uncoupled N atoms separated by considerable molecular mass between these two N atoms. All three of these vibrations would exhibit U−N diatomic isotopic frequency ratios, which are measured as 1.0325, 1.0329, and 1.0327, respectively. Table 1 shows that these three observed bands correlate nicely with the three strongest infrared absorptions computed for the rhombic ring species with two terminal N atoms bonded to the U centers, which is in fact $(NUN)_2$. The ratios of the computed $^{14}N/^{15}N$ frequencies are slightly higher than the observed values owing to harmonic calculations. The higher frequency absorption at 1785 cm^{-1} (Figure S4, ref 14) also gives a mixed isotopic triplet, and its growth on annealing in concert with the above three absorptions suggests a combination band for $(NUN)_2$. Indeed the sum of the 968.0 and 843.8 cm^{-1} modes gives 1811.8 cm^{-1}, which is appropriate for the 1785 cm^{-1} combination band due to cubic anharmonicity. This combination band has considerable intensity which is not surprising for such a molecule as $N(UN)_2N$ with polar bond character. Additionally in the argon matrix samples, these bands shift a few cm^{-1} lower in the direction of the pure nitrogen matrix values on annealing. This is a straightforward process, as diffusion of N_2 molecules on annealing allows for the replacement of Ar atoms thus adding more NN ligands to the rhombic ring system.

Identification of $N(UN)_2$. The 920.6 cm^{-1} band exhibits a similar increase on annealing as the above bands assigned to $(NUN)_2$. It starts out at 925.3 cm^{-1} in our 0.5% N_2 experiment and shifts to 923.1 cm^{-1} on annealing and to 921.8 cm^{-1} with 10% N_2 and to 920.6 cm^{-1} in pure nitrogen. This band shifts to 891.7 cm^{-1} in pure $^{15}N_2$ with the frequency ratio 1.0324, which is satisfactory for a U−N vibration. The computed frequencies for $N(UN)_2$ are also given in Table 1, and the strongest band, the terminal U−N stretching mode, is calculated to be 23 cm^{-1} below this computed band for $(NUN)_2$, and the observed band at 920.6 cm^{-1} is 47.4 cm^{-1} below the 968.0 cm^{-1} band observed for $N(UN)_2N$. This is in reasonably good agreement with calculations, which supports the assignment.

Density Functional Theory. By performing DFT studies along with our experimental results, we can assign the absorptions yielding the IR spectra and associate them with a particular structure and electronic state. In Table 1, we reported the B3LYP vibrational modes for the new species of interest in this work; however, more can be learned from the DFT level of theory. Since these experiments are performed at such low temperatures, only species that are formed by exothermic reactions can be observed. The calculated spectra for assigning the two new products as $(UN)_2$ and $(NUN)_2$ have been discussed, but the energetics for their formation must be explored (structures in Figure 3). The proposed products could be formed via straightforward dimerization reactions (details about active space for CASPT2 and RASPT2 results are in the Electronic Structure and Bonding for (UN)2 and (NUN)2 section detailing the electronic structure of the products):

$$UN + UN \rightarrow (UN)_2 \quad \text{B3LYP, } \Delta E = -146 \text{ kcal/mol}; \quad \text{RASPT2, } \Delta E = -122 \text{ kcal/mol} \tag{6}$$

$$NUN + NUN \rightarrow (NUN)_2 \quad \text{B3LYP, } \Delta E = -64 \text{ kcal/mol}; \quad \text{M06-L, } \Delta E = -70 \text{ kcal/mol}; \quad \text{CCSD(T), } \Delta E = -70 \text{ kcal/mol} \tag{7}$$

Since the NUN concentration in these experiments is much higher than that of UN, the highly exothermic reaction of U

DOI: 10.1021/jacs.5b10458
J. Am. Chem. Soc. 2016, 138, 893−905

and NUN (reaction 8) should be an even more productive source of $(UN)_2$.

$$U + NUN \rightarrow (UN)_2 \quad \text{B3LYP, } \Delta E = -104 \text{ kcal/mol} \tag{8}$$

We also considered the linear molecules NUUN and UNUN as possible products; however, not only were the vibrational modes inconsistent with experiment, but the dimerization reactions were less exothermic: the formation energies of NUUN and NUNU were −73.5 and −107.6 kcal/mol, respectively at the B3LYP level of theory. Alternatively, the following reaction has favorable energetics. The structure of the product is shown in Figure 3.

$$UN + NUN \rightarrow N(UN)_2 \quad \Delta E = -105 \text{ kcal/mol} \tag{9}$$

Reactions 4 and 9 demonstrate that the NUN/UN ring dimer is energetically favorable, further supporting its previously discussed spectroscopic assignment. Furthermore, both the UN and NUN species contain triple bonds, and the manner in which the bonding changes upon dimerization is the focus of the remainder of this manuscript. While these changes can be observed in the vibrational modes (see Table 1), a comparison between the U−N bond distances in the monomers, dimers, and other known uranium nitrogen bonds is given in Table 2 and Figure 3. We can immediately see that upon dimerization the U−N distances in the $(UN)_2$ and $(NUN)_2$ species are longer than in the UN and NUN molecules, respectively. In the dimerization of NUN, one of the U≡N bonds remains a triple bond, while the other is elongated though its interaction with the second NUN group. Mayer bond orders were computed and show that the interaction between the two NUN units is closer to a single bond, while one of the bonds in NUN is reduced to a double bond (Table 2). The weakening of the UN interaction in each NUN group results in a double bond while simultaneously forming a single bond between the two NUN groups. On the other hand, the interaction between two U≡N molecules leads to a drastic change in geometry. In $(UN)_2$, the B3LYP U−N bond lengths are 2.030 Å, much longer than the triple bond in UN of length 1.758 Å. By comparing these bond lengths with those in HN═U≡N, H−U−NH_2, and HN═UH_2, we can tentatively assign the bonds in $(UN)_2$ as between single and double bonds. Furthermore, the bond distances and orders indicate that there is not a direct uranium−uranium bond in either $(NUN)_2$ or $(UN)_2$ (the U−U distance is 3.274 and 3.153 Å and the Mayer bond orders are 0.51 and 0.41, respectively). However, these assignments are based only on bond distances and Mayer bond orders. By performing higher-level calculations and comparing these results to DFT as well as group theory, we can provide deeper insights into the bonding in these species. We also calculated the frequencies and structure for the singlet ground state of the $(NUN)_3$ trimer (Figure S13 and Table S26), which contains a six-membered ring, but found no experimental evidence for this species.

The Bonding in $(UN)_2$: Qualitative Considerations. The high symmetry of D_{2h} diamond-like An_2N_2 complexes makes it attractive for both conceptual and quantitative analysis of their bonding. We will first examine the bonding expected based on group theoretical considerations and our expectations for actinide-ligand bonding. We will then compare these qualitative results to those of quantitative relativistic electronic structure calculations.

There have been numerous previous investigations of the M−M, M−X, and X−X bonding in the M_2X_2 core of ligated transition-metal complexes, i.e., $L_nM(\mu\text{-}X)_2ML_n$, beginning with the seminal work of Shaik et al.[63] and followed by others.[64−66] By comparison, there has been very little examination of the bonding in diamond-like An_2X_2 systems of the actinides, whether ligated or unligated. Schmidt et al. very recently reported the synthesis, structure, and spectroscopic and magnetic characterization of an $[LU(V)]_2(\mu\text{-}O)_2$, where L is a hexadentate (three N, three O) tris(alkoxide)-substituted tetraazacyclononane (**tacn**) ligand.[32] The U centers in this complex have an asymmetric eight-coordination, which makes them less amenable to analysis than the unligated An_2N_2 systems discussed herein. We will focus on the interactions that occur between the An centers and the bridging ligands as well as the different roles played by the An 5f and 6d orbitals.

The reaction of N_2 with two neutral An atoms to form an An_2N_2 complex can be envisioned as a redox process in which six electrons are transferred from the An atoms to the N_2 molecule, leading to a structure best formulated as $[An^{3+}]_2[N^{3-}]_2$ in which the N≡N triple bond is destroyed via the ultimate 3-e^- reduction of each N atom. Each of the N^{3-} ligands has eight valence electrons that can in principle be used in An−N bonding via donation into vacant orbitals on the An atoms. As described above, we believe that $(UN)_2$ is formed here through the straightforward dimerization of two UN molecules or the further reaction of NUN with another U atom in the highly exothermic eqs 6 and 8.

We have previously developed a simple model for describing the bonding in actinide complexes based on two principles: (1) Actinide-ligand bonding preferentially involves the An 6d rather than 5f orbitals, and (2) any formally metal-based electrons on the An center will preferentially reside in the An 5f orbitals.[67] If we apply this model to the An_2N_2 systems, we expect that the major An−N interactions will involve donation from the N^{3-} ligands to vacant 6d orbitals on the An center and that any metal-based electrons on the An(III) center will reside in largely unperturbed 5f orbitals. As we will see, under D_{2h} symmetry, there is an opportune separation of the various interactions that can occur between the An(III) centers and the N^{3-} ligands.

It is convenient to partition the filled orbitals on the two N^{3-} ligands in the way shown in Scheme 1. The 2p orbital on each

Scheme 1. Definition of the Types of N Valence Orbitals in D_{2h} An_2N_2 Complexes

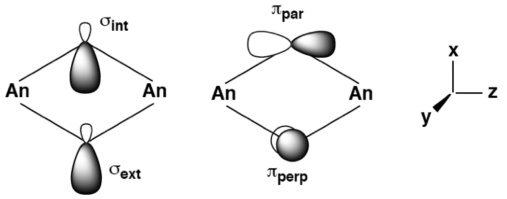

N that points to the center of the diamond has the same symmetry characteristics under D_{2h} as the 2s orbital. We will mix these, essentially creating two sp hybrids on each N, with one pointing at the interior of the diamond (σ_{int}) and one pointing away from the center (σ_{ext}). The remaining two 2p orbitals on each N atom consist of one that lies in the plane of the diamond (π_{par}) and one that is perpendicular to the plane (π_{perp}). Table 3 presents the representations of D_{2h} spanned by

DOI: 10.1021/jacs.5b10458
J. Am. Chem. Soc. 2016, 138, 893−905

Table 3. Representations Spanned by the Ligand and Metal orbitals of An_2N_2 under D_{2h} Symmetry[a]

orbitals	rep.	orbitals	rep.
N σ_{int}, N σ_{ext}	$a_g + b_{3u}$	An 5f[yz^2], 6d[yz]	$b_{3g} + b_{2u}$
N π_{par}	$b_{2g} + b_{1u}$	An 5f[$z(x^2 - y^2)$], 6d[$x^2 - y^2$]	$a_g + b_{1u}$
N π_{perp}	$b_{1g} + b_{2u}$	An 5f[zxy], 6d[xy]	$b_{1g} + a_u$
U 5f[z^3], 6d[z^2]	$a_g + b_{1u}$	An 5f[$x(x^2 - 3y^2)$]	$b_{2g} + b_{3u}$
U 5f[xz^2], 6d[xz]	$b_{2g} + b_{3u}$	An 5f[$y(3x^2 - y^2)$]	$b_{3g} + b_{2u}$

[a]Orbitals that have identical transformation properties are listed together.

these sets of orbitals along with those spanned by the An 5f and 6d orbitals. We see that the symmetry of the molecule leads to a convenient separation of interactions into different representations. For the An centers, orbitals with the same m_l quantum number, such as the 5f[z^3] and the 6d[z^2], have identical transformation properties and are listed together.

The N σ_{ext} orbitals represent essentially outward directed lone pairs on the N atoms and are expected to have only minimal interaction with the An atoms. If our simple model pertains to these diamond structures, then the symmetry-adapted orbitals formed from the filled σ_{int}, π_{par}, and π_{perp} orbitals of the N^{3-} ligands will donate preferentially into appropriate combinations of the 6d orbitals on the An centers. These six ligand combinations separate into distinct representations of D_{2h}, and we can use the allowed symmetry interactions and overlap considerations to predict which An−N interactions will dominate. The expected dominant interactions are sketched schematically in Figure 5. The

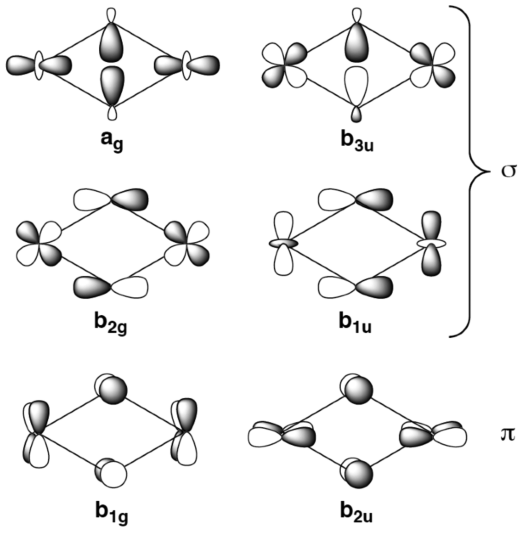

Figure 5. Schematic representation of the expected interactions between the filled valence orbitals of the two N^{3-} ligands and vacant An 6d orbitals in D_{2h} An_2N_2 complexes.

symmetric a_g combination of the N σ_{int} orbitals can, in principle, interact with two of the An 5f and two of the An 6d orbitals. If the interactions with the 6d orbitals are preferred, as we predict, the better overlap will be achieved with the 6d[z^2] orbitals, as shown in Figure 5. Similarly, the b_{1u} combination of the π_{par} orbitals can interact with both the An 6d[z^2] and 6d[$x^2 - y^2$] orbitals. We have depicted the interaction as involving an admixture of these 6d orbitals, producing in essence a set of "6d[x^2]" orbitals.

We note that four of the combinations in Figure 5 (a_g, b_{3u}, b_{2g}, b_{1u}) lie in the plane of the An_2N_2 diamond and will comprise an eight-electron An−N σ framework. The remaining two orbitals (b_{1g} and b_{2u}) form a four-electron π system in the complex. Unlike the π system in cyclobutadiene, both of these π orbitals in An_2N_2 are bonding interactions, facilitated by the phase relationships of the An 6d orbitals. This bonding arrangement is similar to those that we and others have described as metalloaromatic, such as those found in cyclobutadiene metal complexes and metallacyclobutadiene complexes as well as in entirely inorganic systems.[68−70]

The bonding picture that emerges from this qualitative analysis thus accounts for the 16 valence electrons of the two N^{3-} ligands in the following way: Eight electrons are involved in forming the U−N σ framework, four electrons are in the π system of the diamond, and the remaining four electrons are in two essentially lone pairs, one on each N atom. Any remaining metal-based electrons on the An(III) centers are expected to reside in largely unperturbed 5f orbitals. In the case of U_2N_2, we therefore expect that each U center will have three unpaired 5f electrons in addition to those involved in the U−N σ and π bonding. We will now look at how this qualitative description is borne out by the CASSCF calculations.

Electronic Structure and Bonding for $(UN)_2$ and $(NUN)_2$. Both dimers were studied via the RASSCF/RASPT2 approach. In previous work, we have studied the UN and NUN dimers using the complete active space SCF approach (CASSCF/CASPT2) and have demonstrated the importance of properly treating multiconfigurational effects and employed the following active spaces.[14,71] For the UN molecule, we include the 7s, 6d, and 5f orbitals on uranium and the 2p orbitals for nitrogen and their corresponding electrons resulting in a (9,16) active space. If an analogous active space were used for the NUN molecule, an active space of (12,19) orbitals would be included; however, NUN is isoelectronic with the uranyl dication, a closed shell singlet, and only the bonding and antibonding orbitals in the triple bonds need to be included, reducing the active space to (12,12). On the other hand, the natural choice for an active space for the dimers would be to double the active spaces of the monomers. This would leave us with an active space of (18,32) for $(UN)_2$ and (24,24) for $(NUN)_2$. Currently, the largest active space that can typically be treated at the CASSCF level is (16,16), and both of these spaces are well above this limit. The ground state of UN is a quartet. Of the nine active electrons, six are engaged in bonding.

In the $(UN)_2$ dimer, we can anticipate that 12 electrons will engage in bonding and 6 will be localized on the metal centers. This is consistent with our qualitative description insofar as the N 2s orbitals are not included as part of the active space. Likewise, the B3LYP computed spin densities, 3.27 on each U and −0.27 on each N, support this picture. We first ran CASSCF calculations including (6,26) for the lowest septet state of each irreducible representation (D_{2h} symmetry). Only 10 orbitals had occupation numbers higher than 0.02. These orbitals were taken as RAS2 in our RASSCF calculations. The 6 orbitals that including bonding within the $(UN)_2$ ring (and their 12 electrons) were included in RAS1, while their antibonding counterparts were included in RAS3. This leads to an active space of (18,2,2;6,10,6) where the notation of Sauri et al.[72] indicates a RAS space of (n,l,m;i,j,k) where n is the number of electrons in the active space, l is the maximum number of holes in RAS1, and m is the number of electrons

DOI: 10.1021/jacs.5b10458
J. Am. Chem. Soc. 2016, 138, 893−905

allowed in RAS3. Similarly, *i*, *j*, and *k* are the number of orbitals in RAS1, RAS2, and RAS3, respectively. On the other hand, the $(NUN)_2$ dimer does not have any unpaired electrons and, like the NUN molecule, contains two π systems (gerade and the ungerade). The ungerade π orbitals are lower in energy and are put in the inactive space leaving only the six gerade π and corresponding π^* orbitals in the active space resulting in a (12,12) active space for the $(NUN)_2$ dimer. In the dimer, the π orbitals on one of the NUN units mix with the other; however, they do not form a new bonding motif as is the case with $(UN)_2$ (see Figure 6).

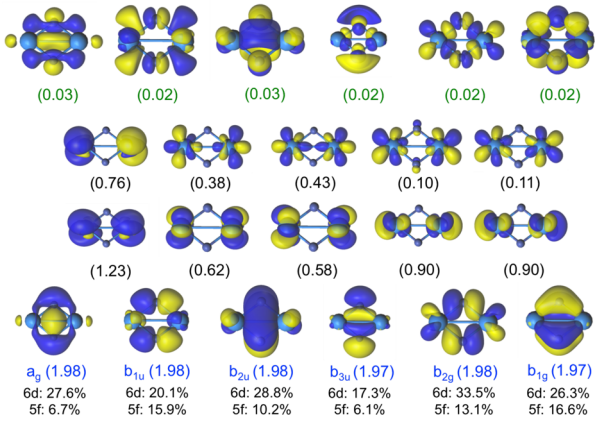

Figure 6. Active natural orbitals from the RASSCF calculation on the $^5B_{1g}$ ground state of $(UN)_2$. Contributions from the 5f and 6d orbitals are given for the six bonding orbitals with occupation numbers close to two. Orbitals in RAS1 are shown with blue occupation numbers in the bottom row, orbitals in RAS2 have black occupation numbers given in the middle rows, and orbitals in RAS3 have green occupation numbers illustrated in the top row.

Based on the qualitative analysis, we would expect that the ground state for $(UN)_2$ would be a septet, corresponding to six unpaired electrons in 5f orbitals. Indeed, at the B3LYP level of theory the ground state is a septet, but lies only 3.2 kcal/mol below the quintet. The RASPT2 ground state is the $^5B_{1g}$ state, which is 3.5 kcal/mol lower in energy than the $^7B_{1u}$ state. The two states differ only in the occupation of the orbitals in RAS2 (those containing the unpaired electrons). Since both states are multiconfigurational in nature, the difference between the two states is not merely one electron flipping from spin up to spin down, but a combination of many effects. One notable difference between two states is that the two molecular orbitals localized on the two U centers with primarily 7s and $6d_{z^2}$ character have a higher occupation number (1.22 and 0.79) in the $^5B_{1g}$ state, while in the $^7B_{2u}$ state, one is singly occupied while the other is empty. The remaining unpaired electrons are distributed among the 5f orbitals (active orbitals are included in Figures 6 and 7).

The bonding within the $(UN)_2$ ring corresponds directly to that predicted by our qualitative analysis: The ring is stabilized by six bonding orbitals involving primarily the 6d orbitals on the uranium centers and the 2p orbitals of the bridging nitrogen atom (see Figure 6). All six bonding orbitals contain contributions from both the 6d and 5f orbitals on the U centers, and two of the orbitals have a 5f contribution only 5% less than that of the 6d. While the contribution of the 5f orbitals is not negligible, orbital mixing alone is not sufficient to determine if this bonding requires 5f orbitals in order to form,

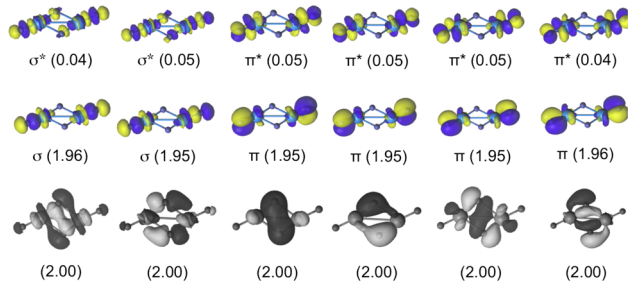

Figure 7. Active natural orbitals (shown in color) from the (12,12) CASSCF calculation on the ^1A_g ground state of $(NUN)_2$. Occupation numbers are given in parentheses. Orbitals in gray (bottom row) are in the inactive space. These are doubly occupied but included since they show the polarization of the orbitals between the two NUN groups.

but it is difficult to assess this by studying the uranium system alone. In order to probe further the role of the f orbitals in the bonding, we have studied a series of metal analogues to determine if this bonding scheme can be observed in the absence of 5f orbitals.

Electronic Structure of $(MN)_2$, Where M = Th, La, Hf, and W. By studying the metal analogues of $(UN)_2$, further insight into the role of the 5f and 6d orbitals in bonding can be obtained. At the DFT level, the optimized geometry for the uranium and metal analogues studied herein is shown in Figure 8. We begin by emphasizing that the bonding in $(UN)_2$,

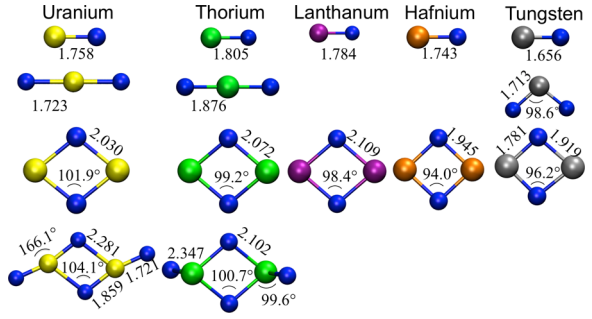

Figure 8. Comparison of select geometric parameters for uranium, thorium, lanthanum, hafnium, and tungsten compounds at determined by B3LYP. Distances are given in Å and angles in degrees. The color scheme is as follows: uranium in yellow, thorium in green, lanthanum in purple, hafnium in orange, tungsten in silver, and nitrogen in blue.

$(ThN)_2$, $(LaN)_2$, and $(HfN)_2$ results in a ring with D_{2h} symmetry, which has been observed in earlier laser ablation experiments,[17,73,74] while the $(WN)_2$ analogue is C_{2v}. In order to rationalize this difference as well as the large change in geometry between $(NUN)_2$ and $(NThN)_2$, we focus on the electronic structure of these systems (See Table 5). The active spaces were chosen in the same fashion as the uranium systems (see Supporting Information for details).

For the $(ThN)_2$ molecule, the bonding is expected to be very similar to that in $(UN)_2$, the only significant difference being the number of unpaired electrons (six for the uranium system but only two for thorium). As in $(UN)_2$, 16 valence electrons are used to build the σ and π frameworks of the $(AnN)_2$ rhombus. The remaining two electrons are expected to remain in Th-based orbitals.[75] We find that the ground state of $(ThN)_2$ is ^1A_g at both the RASPT2 and B3LYP levels of theory. The $^3B_{3u}$ state is 3.3 kcal/mol higher at the B3LYP level of theory and 16.1 kcal/mol higher at the RASPT2 level. The two spin

DOI: 10.1021/jacs.5b10458
J. Am. Chem. Soc. 2016, 138, 893−905

Table 4. Bond Distances and Vibrational Frequencies (Intensities in Parentheses) for Thorium Nitride Species Calculated at the B3LYP Level of Theory[a]

	Th≡N	Th=N	Th−N
ThN	1.805 Å, 991(173)[934][b,c]	–	–
NThN	1.876 Å, 800(55)[757][c]	–	–
$(ThN)_2$	–	2.072 Å, 608(141)[606][c]	–
$(NThN)_2$	–	2.102 Å, 751(575)[n.o.]	2.347 Å, 383(98)[n.o.]
HThN	1.815 Å, 957 [834][d]		
H_2N-ThH			2.176[d]
$HN=ThH_2$		1.951 Å, 826(283)[793][d]	

[a]Distances are in Å, frequencies in cm^{-1}, and intensities in km/mol. Observed argon matrix frequencies are in brackets. [b]Nitrogen matrix frequency 817.2 cm^{-1} for $[NN]_{sat}ThN$. [c]Ref 17. [d]Ref 76.

states differ in the arrangements of the two Th-based electrons in $(ThN)_2$. The ground state is multiconfigurational, but the ^1A_g system contains two orbitals with a significant amount of 7s character (occupation numbers 1.50 and 0.50, while in the analogous triplet, both orbitals are singly occupied). Furthermore, as was the case for $(UN)_2$, the 5f orbitals hybridize with the 6d (percentages are slightly higher (by ∼2−3%) for the Th analogue compared to the values given in Figure 6. Actinide chemists often highlight cases where 5f orbitals engage in bonding, especially when the differences are between the actinides and the remainder of the periodic table, in particular with the lanthanides, can be seen. By studying $(LaN)_2$, we can test if the ability of the 5f orbitals to engage in covalent bonds is essential for the delocalized bonding observed within the rings in $(UN)_2$ and $(ThN)_2$. Our results show that there is a significant decrease in f-orbital contributions to the bonding orbitals, in comparison with the actinides; however, the bonding motif itself contains the same number and type of orbitals in the ring (see Figures S4 and S7 for the $(ThN)_2$ and $(LaN)_2$ orbitals and respective 5f and 6d contributions). This supports our hypothesis that the d orbitals are largely responsible for the bonding in the ring.

The case of $(WN)_2$ provides an interesting test for our qualitative notion of separate roles of the An 5f and 6d orbitals in the $(AnN)_2$ rhombi. Like the $(UN)_2$ system, the $(WN)_2$ molecule has 22 valence electrons. Combinations of the W 5d orbitals along with the N 2s and 2p orbitals can be used to construct orbitals analogous to those in the 16-e^- rhombic framework of the $(UN)_2$ system, i.e., two N-based lone pairs, four W−N σ-framework orbitals, and two W−N π-framework orbitals. In the case of $(WN)_2$, however, we no longer have additional orbitals in which to place the remaining six W-based electrons. This complication is borne out in the calculations: In the $^5B_2$ ground state of $(WN)_2$, the W 5d orbitals must not only engage in bonding in the ring but also hold the unpaired electrons. The competition between these two forces leads to a distortion in the bonds within the $(WN)_2$ ring. On the other hand, turning to the Hf analogue, the bonding in the ring contains the same 16 e^- scheme as the other $(MN)_2$ species, but has two fewer valence electrons per metal center (four in total) than the W systems. Therefore, in this case the ^1A_g ground state adapts the higher symmetry D_{2h} structure once more as the two unpaired electrons occupy natural orbitals that are primarily Hf 6s in character, allowing the Hf 5d to engage in bonding in the ring. See Supporting Information for more details regarding the ground states of these species. We have observed WN and NWN, but not $(WN)_2$, in experiments with tungsten, while rhombic $(ThN)_2$, $(LaN)_2$ and $(HfN)_2$ have been observed in corresponding experiments with Th, La, and Hf.[16,73,74,77] The two ring modes for $(LaN)_2$ shift down 18 cm^{-1} from the argon matrix isolated species to the nitrogen matrix product, which should be saturated with NN ligands, and the two ring modes for $(UN)_2$ shift down comparable amounts, 36 and 12 cm^{-1}, upon changing the matrix host. Finally, the two ring modes for $(HfN)_2$ are observed in solid argon at 682.7 and 775.7 cm^{-1}, but not in solid nitrogen where the $(NN)_xHfN$ complex dominates[65] (shown in gray in Figure 7). This hybridization results in an elongation of the N=UN distance to 1.859 Å and the formation of the U···N interactions (2.281 Å) between subunits. We anticipated that similar bonding would be observed in the Th analogue but were surprised to find the same bonding arise in the ring of $(NThN)_2$, as was observed in the $(UN)_2$ and $(ThN)_2$ rings. Furthermore, the terminal Th−N bonds are much longer (2.347 Å) and are not in the same plane as the $(ThN)_2$ ring (Table 4). In Figure 8, the structure of the NThN dimer is shown, and the Th−N bond distances are very similar to those in $(ThN)_2$. This is drastically different than what was computed for the NUN dimer. In addition the yield of NThN is much less than the yield of NUN in these experiments,[13,14,17] which may be related to the order of magnitude lower exothermicity of reaction 10 relative to reaction 1.

Table 5. Ground-State Symmetries and States for the Systems of Interest in This Work[a]

molecule	point group	B3LYP	CASPT2 (or RASPT2)
UN	$C_{\infty v}$	quartet	^4H
NUN	$D_{\infty h}$	singlet	$^1\Sigma_g^+$
$(UN)_2$	D_{2h}	septet (quintet 3.2)	$^5B_{1g}$ ($^7B_{2u}$ 3.5)
$(NUN)_2$	C_{2h}	singlet	^1A_g
ThN	$C_{\infty v}$	doublet	$^2\Sigma^+$
NThN	$D_{\infty h}$	singlet	$^1\Sigma_g^+$
$(ThN)_2$	D_{2h}	singlet (triplet 3.3)	^1A_g ($^3B_{3u}$ 16.1)
$(NThN)_2$	C_{2h}	singlet	^1A_g
LaN	$C_{\infty v}$	singlet	$^1\Sigma^+$
$(LaN)_2$	D_{2h}	singlet	^1A_g
HfN	$C_{\infty v}$	doublet	$^2\Sigma^+$
$(HfN)_2$	D_{2h}	triplet (singlet 1.7)	^1A_g ($^3B_{3u}$ 7.8)
WN	$C_{\infty v}$	quartet	$^4\Sigma^-$
NWN	C_{2v}	triplet	$^3B_2$
$(WN)_2$	C_{2v}	quintet	$^5B_2$

[a]For $(UN)_2$, $(ThN)_2$, and $(HfN)_2$ another spin state is given in parentheses for comparison since DFT and CASPT2 predict different ground states.

DOI: 10.1021/jacs.5b10458
J. Am. Chem. Soc. 2016, 138, 893−905

$$Th^* + NN \rightarrow NThN \quad B3LYP,\ \Delta E = -5\ kcal/mol \tag{10}$$

$$Th^* + NN \rightarrow N + ThN \quad B3LYP,\ \Delta E = +65\ kcal/mol \tag{11}$$

$$ThN + ThN \rightarrow (ThN)_2 \quad B3LYP,\ \Delta E = -129\ kcal/mol \tag{12}$$

$$NThN + NThN \rightarrow (NThN)_2 \quad B3LYP,\ \Delta E = -100\ kcal/mol \tag{13}$$

Recall that the $(NUN)_2$ and $(UN)_2$ dimers had formation energies of −64 and −146 kcal/mol, respectively, at the B3LYP level of theory. This indicates that in the reactant molecules, the N≡U≡N bonds are stronger than the N≡Th≡N bonds. Furthermore, the insertion of Th* into NN is only exothermic by 5 kcal/mol, whereas the equivalent reaction for uranium was −68 kcal/mol. We propose that ring formation is not strong enough to compensate for breaking the strong bonds of the N≡U≡N group but can do so in the case of N≡Th≡N. This is also supported by the effective bond orders (EBO), computed at the CASSCF level of theory. The EBO is the sum of the occupation numbers (number of electrons per bond) of the occupied bonding orbitals minus the sum of the occupation numbers of antibonding orbitals divided by two. The EBO is 2.87 for NUN, while for NThN the bonding is slightly weaker with an EBO of 2.61.

CONCLUSIONS

The $(UN)_2$ and $(NUN)_2$ molecules have been formed via matrix isolation spectroscopy, and their electronic structure has been characterized using high-level wave function-based methods. These novel cyclic dimers, $(UN)_2$ and $(NUN)_2$, exhibit complex electronic structures. Most notably, we have determined that the interactions between two N≡U≡N units is favorable and reduces one N≡U bond per molecule to a double bond while forming a single bond between the two dimers. On the other hand, the interaction between two U≡N units results in the formation of four σ and two delocalized π orbitals with contributions primarily from the uranium 6d and nitrogen 2p orbitals. Furthermore, the thorium, lanthanum, and hafnium analogues show the same bonding scheme within the $(MN)_2$ ring. This supports the hypothesis that the d orbitals are responsible for the bonding, while the 5f orbitals hold the unpaired electrons. On the other hand, in the $(WN)_2$ species the d orbitals must hold the unpaired electrons while engaging in bonding within the ring. This competition leads to a reduction in symmetry within the ring from D_{2h} to C_{2v}. Finally, the strong bonds in the N≡U≡N molecule are not broken in favor of ring formation in the $(NUN)_2$ dimer, but the weaker N≡Th≡N bonds are modified in the $(NThN)_2$ dimer, which contains an internal $(ThN)_2$ ring similar to $(ThN)_2$ itself.

ASSOCIATED CONTENT

Supporting Information

The Supporting Information is available free of charge on the ACS Publications website at DOI: 10.1021/jacs.5b10458.

Additional discussion of the active space, active orbitals, optimized geometries, and energies of calculated electronic states (PDF)

AUTHOR INFORMATION

Corresponding Authors

*bessvlai@gmail.com
*lsa@virgina.edu

Notes

The authors declare no competing financial interest.

ACKNOWLEDGMENTS

Dedicated to the memory of our good friend and colleague Professor Malcolm H. Chisholm (1945−2015), whose fundamental studies of the structure and bonding in metal−metal bonding have taught us so much. L.A. gratefully acknowledges financial support from DOE grant no. DE-SC0001034. X.-F.W. is grateful for support from NSFC grant 21173158.

REFERENCES

(1) Silva, G. W. C.; Yeamans, C. B.; Sattelberger, A. P.; Hartmann, T.; Cerefice, G. S.; Czerwinski, K. R. *Inorg. Chem.* **2009**, *48* (22), 10635−10642.
(2) Silva, C. M.; Hunt, R. D.; Snead, L. L.; Terrani, K. A. *Inorg. Chem.* **2015**, *54*, 293−298.
(3) Hayton, T. W. *Chem. Commun.* **2013**, *49* (29), 2956−2973.
(4) Andrews, L.; Wang, X.; Lindh, R.; Roos, B. O.; Marsden, C. J. *Angew. Chem., Int. Ed.* **2008**, *47* (29), 5366−5370.
(5) Wang, X.; Andrews, L.; Marsden, C. J. *Chem. - Eur. J.* **2008**, *14* (30), 9192−9201.
(6) Lyon, J. T.; Andrews, L.; Malmqvist, P. Å.; Roos, B. O.; Yang, T.; Bursten, B. E. *Inorg. Chem.* **2007**, *46* (12), 4917−4925.
(7) Wang, X.; Andrews, L.; Vlaisavljevich, B.; Gagliardi, L. *Inorg. Chem.* **2011**, *50* (8), 3826−3831.
(8) Hunt, R. D.; Andrews, L. *J. Chem. Phys.* **1993**, *98* (5), 3690−3696.
(9) Zhou, M.; Andrews, L.; Li, J.; Bursten, B. E. *J. Am. Chem. Soc.* **1999**, *121* (41), 9712−9721.
(10) Zhou, M.-F.; Andrews, L.; Ismail, N.; Marsden, C. *J. Phys. Chem. A* **2000**, *104*, 5495−5502.
(11) Gabelnick, S. D.; Reedy, G. T.; Chasanov, M. G. *J. Chem. Phys.* **1973**, *58* (2), 4468−4475.
(12) Hunt, R. D.; Yustein, J. T.; Andrews, L. *J. Chem. Phys.* **1993**, *98* (8), 6070−6074.
(13) Andrews, L.; Wang, X.; Gong, Y.; Vlaisavljevich, B.; Gagliardi, L. *Inorg. Chem.* **2013**, *52*, 9989−9993.
(14) Andrews, L.; Wang, X.; Gong, Y.; Kushto, G. P.; Vlaisavljevich, B.; Gagliardi, L. *J. Phys. Chem. A* **2014**, *118* (28), 5289−5303.
(15) Gagliardi, L.; La Manna, G.; Roos, B. O. *Faraday Discuss.* **2003**, *124*, 63.
(16) Green, D. W.; Reedy, G. T. *J. Chem. Phys.* **1976**, *65* (7), 2921−2922.
(17) Kushto, G. P.; Souter, P. F.; Andrews, L. *J. Chem. Phys.* **1998**, *108* (2), 7121−7130.
(18) Gagliardi, L.; Roos, B. O. *Chem. Phys. Lett.* **2000**, *331*, 229−234.
(19) Roos, B. O.; Lindh, R.; Cho, H.-G.; Andrews, L. *J. Phys. Chem. A* **2007**, *111*, 6420−6424.
(20) Matthew, D. J.; Morse, M. D. *J. Chem. Phys.* **2013**, *138* (18), 184303.
(21) Heaven, M. C.; Barker, B. J.; Antonov, I. O. *J. Phys. Chem. A* **2014**, *118*, 10867−10881.
(22) King, D. M.; Tuna, F.; McInnes, E. J. L.; McMaster, J.; Lewis, W.; Blake, A. J.; Liddle, S. T. *Nat. Chem.* **2013**, *5* (6), 482−488.
(23) King, D. M.; Tuna, F.; McInnes, E. J. L.; McMaster, J.; Lewis, W.; Blake, A. J.; Liddle, S. T. *Science* **2012**, *337*, 717−720.
(24) Cleaves, P. A.; King, D. M.; Kefalidis, C. E.; Maron, L.; Tuna, F.; Mcinnes, E. J. L.; Mcmaster, J.; Lewis, W.; Blake, A. J.; Liddle, S. T. *Angew. Chem., Int. Ed.* **2014**, *53*, 10412−10415.
(25) Burns, C. J. *Science* **2005**, *309* (5742), 1823−1824.

DOI: 10.1021/jacs.5b10458
J. Am. Chem. Soc. 2016, 138, 893−905

(26) Evans, W. J.; Kozimor, S. A.; Ziller, J. W. *Science* **2005**, *309* (5742), 1835−1838.
(27) Hayton, T. W.; Boncella, J. M.; Scott, B. L.; Palmer, P. D.; Batista, E. R.; Hay, P. J. *Science* **2005**, *310* (5756), 1941−1943.
(28) Ephritikhine, M. *Dalton Trans.* **2006**, *21*, 2501−2516.
(29) Cantat, T.; Arliguie, T.; Noël, A.; Thuéry, P.; Ephritikhine, M.; Floch, P.; Mézailles, N. *J. Am. Chem. Soc.* **2009**, *131* (3), 963−972.
(30) Fox, A. R.; Arnold, P. L.; Cummins, C. C. *J. Am. Chem. Soc.* **2010**, *132* (10), 3250−3251.
(31) Roussel, P.; Scott, P. *J. Am. Chem. Soc.* **1998**, *120* (5), 1070−1071.
(32) Schmidt, A.-C.; Heinemann, F. W.; Lukens, W. W.; Meyer, K. *J. Am. Chem. Soc.* **2014**, *136*, 11980−11993.
(33) Andrews, L.; Cho, H. G. *Organometallics* **2006**, *25* (17), 4040−4053.
(34) Becke, A. D. *J. Chem. Phys.* **1993**, *98* (7), 5648−5652.
(35) Lee, C.; Yang, W.; Parr, R. G. *Phys. Rev. B: Condens. Matter Mater. Phys.* **1988**, *37* (2), 785−789.
(36) Frisch, M. J.; Pople, J. a.; Binkley, J. S. *J. Chem. Phys.* **1984**, *80* (7), 3265−3269.
(37) Küchle, W.; Dolg, M.; Stoll, H.; Preuss, H. *J. Chem. Phys.* **1994**, *100* (10), 7535−7542.
(38) Mayer, I. *Chem. Phys. Lett.* **1983**, *97* (3), 270−274.
(39) Mayer, I. *Int. J. Quantum Chem.* **1984**, *26*, 151−154.
(40) Zhao, Y.; Truhlar, D. G. *J. Chem. Phys.* **2006**, *125*, 194101.
(41) Frisch, M. J.; Trucks, G. W.; Schlegel, H. B.; Scuseria, G. E.; Robb, M. A.; Cheeseman, J. R.; Scalmani, G.; Barone, V.; Mennucci, B.; Petersson, G. A.; Nakatsuji, H.; Caricato, M.; Li, X.; Hratchian, H. P.; Izmaylov, A. F.; Bloino, J.; Zheng, G.; Sonnenberg, J. L.; Hada, M.; Ehara, M.; Toyota, K.; Fukuda, R.; Hasegawa, J.; Ishida, M.; Nakajima, T.; Honda, Y.; Kitao, O.; Nakai, H.; Vreven, T.; Montgomery, J. A., Jr.; Peralta, J. E.; Ogliaro, F.; Bearpark, M.; Heyd, J. J.; Brothers, E.; Kudin, K. N.; Staroverov, V. N.; Kobayashi, R.; Normand, J.; Raghavachari, K.; Rendell, A.; Burant, J. C.; Iyengar, S. S.; Tomasi, J.; Cossi, M.; Rega, N.; Millam, J. M.; Klene, M.; Knox, J. E.; Cross, J. B.; Bakken, V.; Adamo, C.; Jaramillo, J.; Gomperts, R.; Stratmann, R. E.; Yazyev, O.; Austin, A. J.; Cammi, R.; Pomelli, C.; Ochterski, J. W.; Martin, R. L.; Morokuma, K.; Zakrzewski, V. G.; Voth, G. A.; Salvador, P.; Dannenberg, J. J.; Dapprich, S.; Daniels, A. D.; Farkas, Ö.; Foresman, J. B.; Ortiz, J. V.; Cioslowski, J.; Fox, D. J. *Gaussian 09*, Revision D.01; Gaussian, Inc.; Wallingford, CT, 2009.
(42) Roos, B. O.; Taylor, P. R.; Siegbahn, P. E. M. *Chem. Phys.* **1980**, *48* (2), 157−173.
(43) Andersson, K.; Malmqvist, P.; Roos, B.; Sadlej, A. J.; Wolinskit, K. *J. Phys. Chem.* **1990**, *94*, 5483−5488.
(44) Andersson, K.; Malmqvist, P.-A.; Roos, B. O. *J. Chem. Phys.* **1992**, *96* (2), 1218−1226.
(45) Malmqvist, P.; Rendell, A.; Roos, B. *J. Phys. Chem.* **1990**, *94*, 5477−5482.
(46) Malmqvist, P. A.; Pierloot, K.; Shahi, A. R. M.; Cramer, C. J.; Gagliardi, L. *J. Chem. Phys.* **2008**, *128* (20), 204109.
(47) Douglas, M.; Kroll, N. M. *Ann. Phys. (Amsterdam, Neth.)* **1974**, *82* (1), 89−155.
(48) Hess, B. A. *Phys. Rev. A: At., Mol., Opt. Phys.* **1986**, *33* (6), 3742−3748.
(49) Roos, B. O.; Lindh, R.; Malmqvist, P. Å.; Veryazov, V.; Widmark, P. O. *J. Phys. Chem. A* **2004**, *108* (15), 2851−2858.
(50) Roos, B. O.; Lindh, R.; Malmqvist, P. Å.; Veryazov, V.; Widmark, P. O. *J. Phys. Chem. A* **2005**, *109* (29), 6575−6579.
(51) Aquilante, F.; De Vico, L.; Ferre, N.; Ghigo, G.; Malmqvist, P.-A.; Neogrady, P.; Pedersen, T. B.; Pitonak, M.; Reiher, M.; Roos, B. O.; Serrano-Andres, L.; Urban, M.; Veryazov, V.; Lindh, R. *J. Comput. Chem.* **2010**, *31* (1), 224−247.
(52) Aquilante, F.; Pedersen, T. B.; Lindh, R. *J. Chem. Phys.* **2007**, *126*, 194106.
(53) Aquilante, F.; Lindh, R.; Pedersen, T. B. *J. Chem. Phys.* **2008**, *129*, 034106.
(54) Aquilante, F.; Malmqvist, P. Å.; Pedersen, T. B.; Ghosh, A.; Roos, B. O. *J. Chem. Theory Comput.* **2008**, *4* (5), 694−702.
(55) Aquilante, F.; Gagliardi, L.; Pedersen, T. B.; Lindh, R. *J. Chem. Phys.* **2009**, *130*, 154107.
(56) Peterson, K. A. *J. Chem. Phys.* **2015**, *142* (7), 074105.
(57) Knowles, P. J.; Hampel, C.; Werner, H.-J. *J. Chem. Phys.* **1993**, *99*, 5219−5227.
(58) Werner, H.-J.; Knowles, P. J.; Knizia, G.; Manby, F. R.; Schütz, M.; Celani, P.; Korona, T.; Lindh, R.; Mitrushenkov, A.; Rauhut, G.; Shamasundar, K. R.; Adler, T. B.; Amos, R. D.; Bernhardsson, A.; Berning, A.; Cooper, D. L.; Deegan, M. J. O.;Dobbyn, A. J.; Eckert, F.; Goll, E.; Hampel, C.; Hesselmann, A.; Hetzer, G.; Hrenar, T.; Jansen, G.; Koppl, C.; Liu, Y.; Lloyd, A. W.; R. A. Mata, R. A.; May, A. J.; McNicholas, S. J.; Meyer, W.; Mura, M. E.; Nicklass, A.; O'Neill, D. P.; Palmieri, P.; Peng, D.; Pfluger, K.; Pitzer, R.; Reiher, M.; Shiozaki, T.; Stoll, H. Stone, A. J.; Tarroni, R.; Thorsteinsson, T.; Wang, M. *Molpro, a Package of Ab Initio Programs*, Version 2012.1; Molpro: Cardiff, U.K., 2012.
(59) Andrews, L.; Wang, X.; Gong, Y.; Vlaisavljevich, B.; Gagliardi, L. *Inorg. Chem.* **2013**, *52* (17), 9989−9993.
(60) Tian, R.; Facelli, J. C.; Michl, J. *J. Phys. Chem.* **1988**, *92* (14), 4073−4079.
(61) White, D.; Seshadri, K. S.; Dever, D. F.; Mann, D. E.; Linevsky, M. J. *J. Chem. Phys.* **1963**, *39* (10), 2463−2473.
(62) Wang, X.; Andrews, L.; Li, J.; Bursten, B. E. *Angew. Chem., Int. Ed.* **2004**, *43* (19), 2554−2557.
(63) Shaik, S.; Hoffmann, R.; Fisel, C. R.; Summerville, R. H. *J. Am. Chem. Soc.* **1980**, *102* (14), 4555−4572.
(64) Palacios, A. A.; Aullón, G.; Alemany, P.; Alvarez, S. *Inorg. Chem.* **2000**, *39* (15), 3166−3175.
(65) Zurek, J. M.; Paterson, M. J. *Inorg. Chem.* **2009**, *48* (22), 10652−10657.
(66) Chiarella, G. M.; Cotton, F. A.; Murillo, C. a.; Zhao, Q. *Inorg. Chem.* **2014**, *53* (4), 2288−2295.
(67) Bursten, B. E.; Palmer, E. J.; Sonnenberg, J. L. *On the Role of F-Orbitals in the Bonding in F-Element Complexes: The "FEUDAL" Model as Applied to Organoactinide and Actinide Aquo Complexes*; May, I., Bryan, N. D., Alvares, R., Eds.; Special Publications; The Royal Society of Chemistry: London, 2006.
(68) Bursten, B. E.; Fenske, R. F. *Inorg. Chem.* **1979**, *18* (7), 1760−1765.
(69) Bursten, B. E. *J. Am. Chem. Soc.* **1983**, *105* (1), 121−122.
(70) Boldyrev, A. I.; Wang, L. S. *Chem. Rev.* **2005**, *105* (10), 3716−3757.
(71) Vlaisavljevich, B.; Gagliardi, L.; Wang, X.; Liang, B.; Andrews, L.; Infante, I. *Inorg. Chem.* **2010**, *49* (20), 9230−9235.
(72) Sauri, V.; Serrano-Andrés, L.; Shahi, A. R. M.; Gagliardi, L.; Vancoillie, S.; Pierloot, K. *J. Chem. Theory Comput.* **2011**, *7* (1), 153−168.
(73) Chertihin, G.; Bare, W. D.; Andrews, L. *J. Phys. Chem. A* **1998**, *102*, 3697−3704.
(74) Kushto, G. P.; Souter, P. F.; Chertihin, G. V.; Andrews, L. *J. Chem. Phys.* **1999**, *110* (18), 9020−9031.
(75) Bursten, B. E.; Rhodes, L. F.; Strittmatter, R. J. *J. Am. Chem. Soc.* **1989**, *111* (8), 2756−2758.
(76) Wang, X.; Andrews, L.; Marsden, C. J. *Chem. - Eur. J.* **2007**, *13* (19), 5601−5606.
(77) Andrews, L.; Souter, P. F.; Bare, W. D.; Liang, B. *J. Phys. Chem. A* **1999**, *103*, 4649−4658.

DOI: 10.1021/jacs.5b10458
J. Am. Chem. Soc. 2016, 138, 893−905